Results in Physics 57 (2024) 107424

Contents lists available at ScienceDirect

Results in Physics

journal homepage: www.elsevier.com/locate/rinp

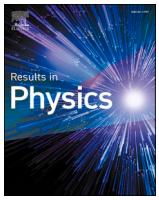

Impact of five obstacles with constant temperatures on the mixed convection flow of water/copper nanofluid in a rectangular cavity with a magnetic field

Jawed Mustafa [a,*], Saeed Alqaed [a], Shahid Husain [b], Mohsen Sharifpur [c,d,*]

[a] Mechanical Engineering Department, College of Engineering, Najran University, P.O. Box (1988), Najran 61441, Saudi Arabia
[b] Department of Mechanical Engineering, Zakir Husain College of Engineering and Technology, Aligarh Muslim University, Aligarh 202002, India
[c] Department of Mechanical and Aeronautical Engineering, University of Pretoria, South Africa
[d] Department of Medical Research, China Medical University Hospital, China Medical University, Taichung, Taiwan

ARTICLE INFO

Keywords:
Mixed convection flow
Nanofluid
LBM
Magnetic field
Hot obstacles

ABSTRACT

In this research, we conduct a computational investigation into the mixed convection flow of copper/water nanofluids (NFs) within a rectangular cavity, utilizing the Lattice Boltzmann Method (LBM). The cavity is uniquely configured with five high-temperature obstructions (HOBs), and we vary their dimensions and positions to evaluate Nusselt numbers (Nu) across a range of Richardson numbers (Ri). The three walls of the cavity, excluding the moveable top wall, are thermally insulated, while the latter is maintained at a lower temperature. A constant magnetic field (MCF) exerts influence within the cavity, with Ri spanning from 0.01 to 100, HOBs ranging from 0.1 to 0.5, and HOBs at the bottom wall spanning from 0.25 to 0.4. This numerical investigation is executed using a customized in-house code, focusing on examining heat transfer (HTR) dynamics within the cavity. Our findings reveal that augmenting the height of the HOBs and positioning them closer to the cold wall significantly enhances the average Nusselt number (Nu_{av}). Conversely, an increase in Ri leads to a reduction in Nu_{av} on the cold wall. Specifically, the most notable enhancement, with a 66.7 % increase in Nu_{av}, occurs at Ri = 0.01 when HOBs are elevated from 0.1 to 0.5. On the other hand, an increment in Ri from 0.01 to 100 results in a 79.4 % reduction in Nu_{av}. Furthermore, elevating the HOBs from 0.25 to 0.4 produces a substantial 44.3 % increase in Nu_{av}.

Introduction

In the past two decades, the Lattice Boltzmann Method (LBM) has emerged as a powerful numerical tool for the analysis of complex fluid flows [1,2]. This innovative approach, born from the foundation of the lattice gas cellular automata and the gas-kinetic BGK scheme, has significantly advanced our understanding and simulation of fluid dynamics [3]. LBM's distinctiveness lies in its microscopic perspective, where fluid distribution functions form the fundamental framework for the analysis of fluid flow behaviors [4,5]. Instead of directly solving the intricate and nonlinear Navier-Stokes equations, LBM opts for a unique path by solving the simplified and quasi-linear Boltzmann transport equation using distribution functions that signify the probability of locating fluid particles at specific positions [6]. The origins of the Lattice Boltzmann Method can be traced back to 1952 when Frisch et al. [7] introduced a numerical solution for the Boltzmann equation. Subsequent developments by McNamara and Zanetti, Higora and Higuera [8], and Chen et al. [9] refined and expanded this method, opening up possibilities for its application in diverse domains of fluid dynamics. However, despite its versatility, the LBM has seen comparatively fewer applications in simulating the flow and heat transfer phenomena of nanofluids (NFs) in scenarios characterized by the concurrent presence of a magnetic field (MCF) and a porous medium [10].

It has been discovered that considering internal heat production in the base fluid affects the temperature field more than the flow field. Asadi et al. [11] used LBM to investigate the fluid flow and forced convection HTR inside of a two-dimensional horizontal channel with and without obstructions. To boost the pace of HTR and increase the

* Corresponding authors at: Mechanical Engineering Department, College of Engineering, Najran University, Najran, Saudi Arabia (J. Mustafa) and Department of Mechanical and Aeronautical Engineering, University of Pretoria, South Africa (M. Sharifpur).
E-mail addresses: jmmustafa@nu.edu.sa (J. Mustafa), mohsen.sharifpur@up.ac.za (M. Sharifpur).

https://doi.org/10.1016/j.rinp.2024.107424
Received 1 May 2023; Received in revised form 20 January 2024; Accepted 29 January 2024
Available online 30 January 2024

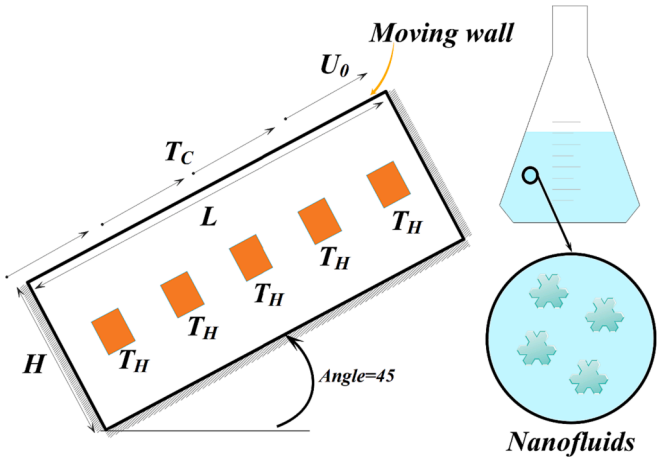

Fig. 1. The cavity with water/Cu NFs.

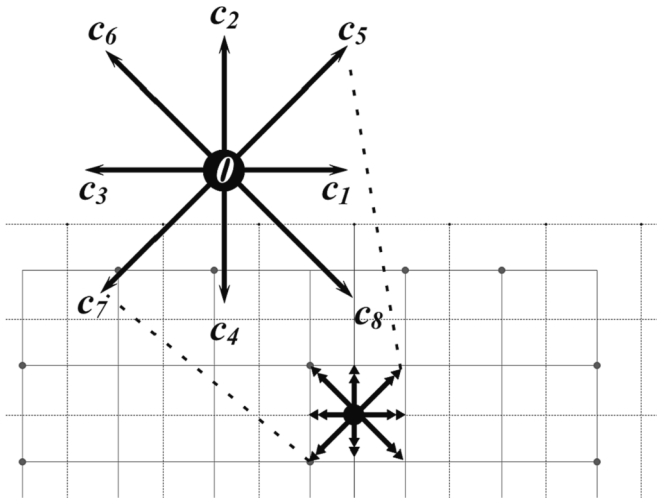

Fig. 2. Discrete velocity vectors for the D2Q9 model.

amount of thermal energy inside the channel, many different barrier configurations were considered for the flow field and HTR. According to the findings, replacing standard NFs with hybrid NFs leads to an increase in the HTR rate inside the channel. With a rise in, Nu also rose (1.17 times). It has been shown that the kind of barrier arrangement and the sort of NFs may both potentially have a significant impact on the characteristics of the flow field and the HTR in the channel. As a result of this work, a platform has been created for using LBM to evaluate fluid flow past discrete barriers. HTR fluid may be any fluid, including water, air, ethylene glycol, and others [12]. NFs are a fluid that has been of great interest to researchers and HTR devices in recent years [13]. NFs are prepared by mixing different NPs and different fluids such as water, ethylene glycol, oil, etc. [14]. One of the heat exchange devices researchers use is cavities in which natural, forced or mixed convection occurs [15]. Magnetic hydrodynamics is a relatively new branch of fluid dynamics. This branch of the subject of fluids comes up when the electrically conductive fluid has motion and is affected by the magnetic field [16]. Simultaneously, applying magnetic fields has proven to be an effective tool for manipulating fluid flow dynamics and, consequently, heat transfer processes [17].

Zhou et al. [18] investigated the convective heat transfer of a nano-fluid in a two-phase scenario. They placed triangular blades at the bottom of a cavity and examined the effect of a magnetic field on the convective flow of the nano-fluid around them. Their results indicated that the Bejan number reaches its maximum value when the length of the blades is in the most extended state. The highest entropy levels were generated at the lowest height of the left barrier and the highest height of the middle barrier.

Ketchate et al. [19] also delved into the stability and analysis of a Newtonian nano-fluid in the context of forced convective heat transfer. They examined the flow of a nano-fluid within a channel under the influence of a magnetic field and radiation effects. Their results showed that introducing nanoparticles into the base fluid increases the fluid's inertia, reducing disturbances. Among various geometric shapes of nanoparticles, blade-like shapes have a more significant stabilizing effect on the convective heat transfer. Parameters like the Prandtl and Richardson numbers maintain stability in forced convective heat transfer. Furthermore, the magnetic field, thermal radiation, and the permeability of the porous medium all affect the stability of forced convective heat transfer and have stabilizing effects.

Abderrahmane et al. [20] studied the influence of an adiabatic rotating inner cylinder within a cavity on the forced convective heat transfer of a hybrid nano-fluid. Using the power-law model, they assumed two-dimensional, incompressible, steady, and adiabatic conditions for the governing equations of the non-Newtonian hybrid nano-fluid. They numerically solved these equations and found that the results indicate that a constant rotation of the cylinder in the opposite direction of clockwise motion increases forced convective heat transfer, while its rotation in the clockwise direction has the opposite effect. Moreover, heat transfer is enhanced when the cylinder approaches the hot wall in the counterclockwise direction.

Akhter et al. [21] also numerically examined two non-smooth cylinders in rotational motion within a rectangular cavity in the presence of an external magnetic field. Their results showed that increasing the heat transfer rate decreases with increasing magnetic field strength. The lowest heat transfer rate occurs with the highest magnetic field intensity. The presence of triangular rough elements enhances fluid flow and heat transfer significantly.

In the ever-evolving field of heat transfer and fluid dynamics, recent years have witnessed a growing interest in innovative techniques to enhance heat transfer efficiency, with particular attention to the applications of nanofluids (NFs), magnetic fields and controlled boundary conditions [22]. Among the intriguing directions of inquiry within this domain, the deployment of five obstacles, each maintained at constant temperatures, within a rectangular cavity to influence the mixed convection flow of water/copper NFs has emerged as a captivating study area. NFs, which consist of nanoparticles suspended in a base fluid, offer remarkable thermal properties and have been extensively explored for their potential to augment heat transfer [23]. Concurrently, applying magnetic fields has demonstrated the ability to manipulate fluid flow characteristics, introducing new avenues for enhancing heat transfer processes. The amalgamation of these factors presents an innovative and complex system where the interaction of five temperature-controlled obstacles and a magnetic field can lead to unique phenomena in mixed convection heat transfer. This research paper delves into the numerical exploration of a cavity hosting water/copper NFs convection. The cavity features a dynamic wall to induce convection flow, while a constant magnetic field influences the domain. We introduce five high-temperature obstructions strategically positioned in the cavity's center. Through systematic manipulations of their dimensions and locations, we conduct simulations utilizing the Lattice Boltzmann Method (LBM) across various Richardson numbers (Ri). The culmination of our investigation offers valuable insights through visualizing velocity and temperature contours, alongside quantifying Nusselt numbers (Nu) and average Nusselt numbers (Nuav).

Problem definition

The rectangular cavity has a width of l and a length of 5 l. In the center of the hollow, five obstructions have a high T_H temperature. The cavity's bottom and side walls are highly insulated, while its top wall is

Table 1
Thermophysical properties of base fluid and NPs [30].

Property	Cu	H_2O
$c_p\left(Jkg^{-1}K^{-1}\right)$	385	4179
$\rho\left(kgm^{-3}\right)$	8933	997.1
$k\left(Wm^{-1}K^{-1}\right)$	401	0.613
$\beta\left(K^{-1}\right)$	1.67×10^{-5}	21×10^{-5}
μ(Pa·s)	–	0.001003
d(nm)	100	–

Table 2
Comparison of Nu_{av} at Ri = 0.01 and 100 for the grids with various grid points.

Ri	18,000	24,500	32,000	40,500	50,000	60,500
0.01	12.65	11.97	11.68	11.51	11.44	11.43
100	2.89	2.73	2.59	2.41	2.35	2.35

Table 3
The amounts of Nu_{av} were calculated on the hot wall.

Ha	Ref. [31]	Present work	%Eror
0	12.23	12.06	1.4 %
50	12.75	12.41	2.6 %
100	13.18	12.71	3.2 %

just T_C below ambient. The constant U_0 velocity of this wall forces forced convection flow inside the hollow. Their distance from the bottom wall H is altered from 0.25 to 0.4, and the HOB is adjusted from 0.1 to 0.5. (Fig. 1). The cavity and NFs are subjected to an MCF with an applied Hartmann number (Ha) of 20.

Governing equations

Two distribution functions are used in the work being described here for the flow and temperature fields. When applied to a macroscopic scale, these distribution functions fulfill the continuity, momentum, and energy equations. Both of these fields will make use of the D2Q9 grid layout. The configuration of this particular kind of lattice is seen in Fig. 2. Several sources have provided information on the specifics of this arrangement as well as the benefits that it offers. [24].

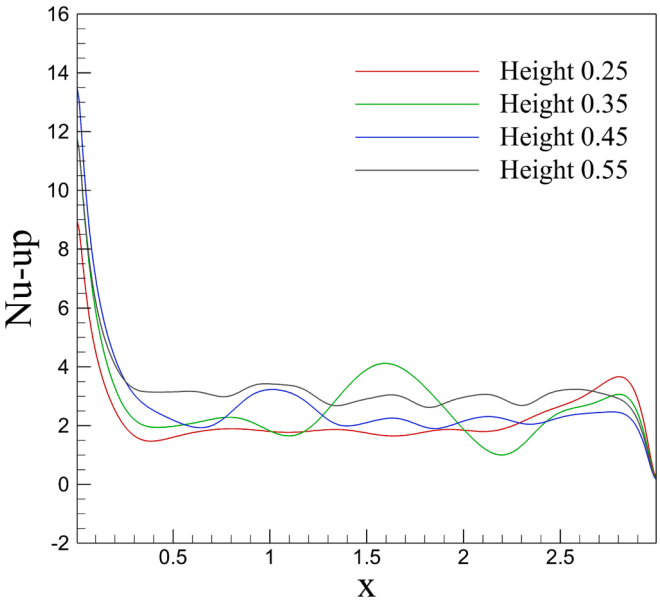

Fig. 4. The value of the local Nu on the upper wall for different HOBs.

Table 4
Shows the values of Nu_{av} on the top wall for different HOBs.

H = 0.25	2.23
H = 0.30	2.65
H = 0.35	2.70
H = 0.40	3.22

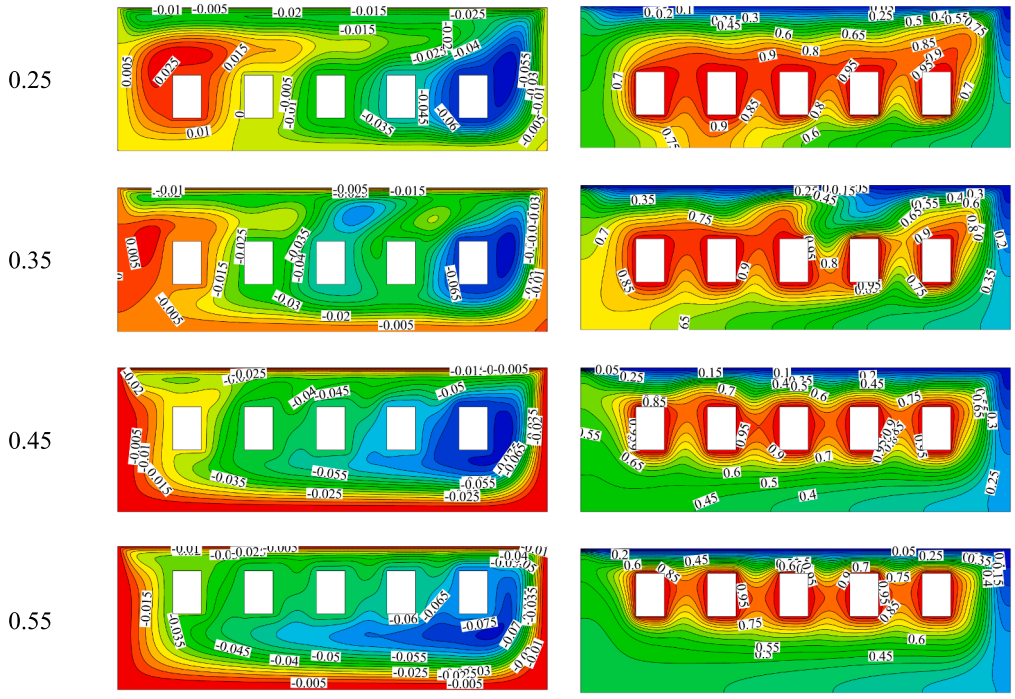

Fig. 3. The contours of streamlines and isotherms for different HOBs.

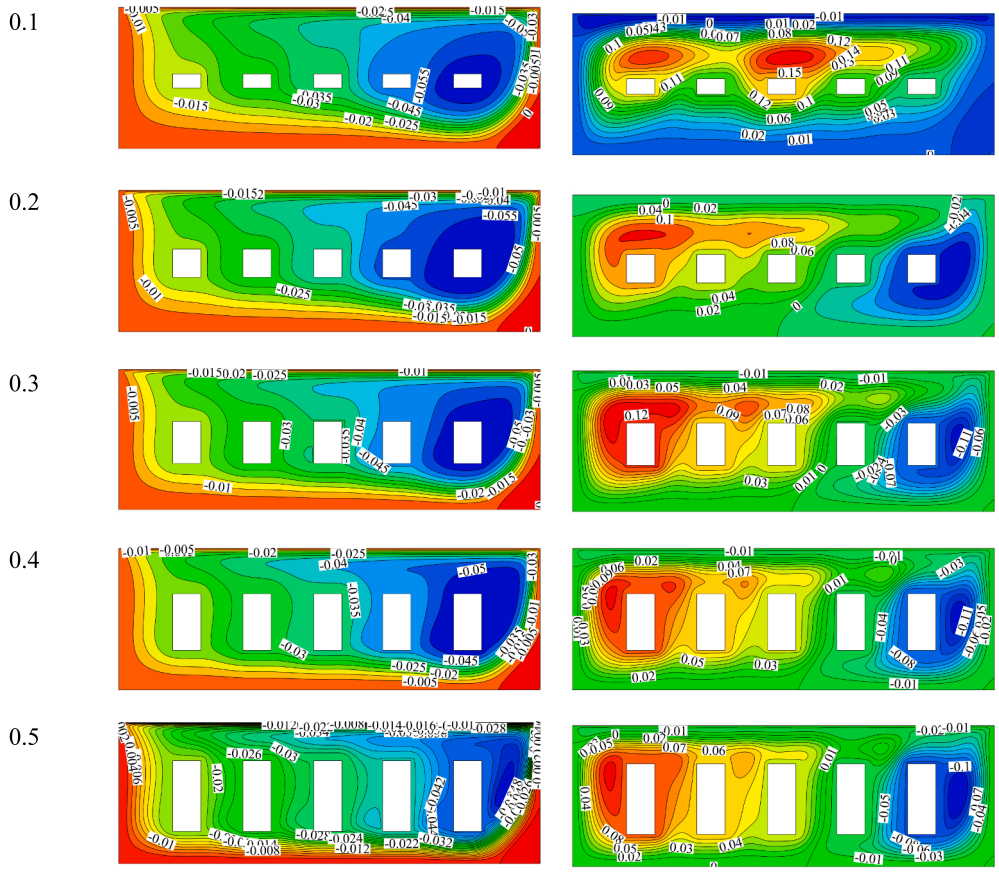

Fig. 5. The contours of the streamlines for different HOBs and various values of Ri.

Assumptions:

1- The flow is two-dimensional and laminar, 2- The flow regime is incompressible, 3- The fluid is Newtonian, 4- Radiative HTR and viscous loss are negligible, and 5- Boussinesq approximation is used.

The lattice Boltzmann equations for the flow and temperature fields are represented as Eqs. (1) and (2), respectively, when there is an external force present [25]. Equations (3) and (4), which are used in the D2Q9 model, provide the equilibrium distribution functions for the flow and temperature fields, respectively. Equation (5) expresses the equation for the macroscopic quantities. Equations (6) and (7) describe the weight coefficients and discrete velocities, respectively (7). According to Eq. (1), the influence of magnetic and buoyancy forces is considered as a source term (8). In Eq. (9), the relaxation time for the flow and temperature fields (10), as well as the dimensionless variables utilized in the equations to illustrate the conclusions, are provided [26].

$$f_i(x+c_i\Delta t, t+\Delta t) = f_i(x,t) - \frac{\Delta t}{\tau_v}\left[(f_i(x,t) - f_i^{eq}(x,t)\right] + \Delta t c_i F_i \tag{1}$$

$$g_i(x+c_i\Delta t, t+\Delta t) = g_i(x,t) - \frac{\Delta t}{\tau_c}[(g_i(x,t) - g_i^{eq}(x,t)] + \left(Q/\rho C_p\right)_{nf}\Big(T - T_c\Big) \tag{2}$$

$$f_i^{(eq)} = \omega_i\left[1 + \frac{(C_i.u)}{C_s^2} - \frac{1}{2C_s^2}(u.u) + \frac{1}{2}\frac{(C_i.u)^2}{C_s^4}\right] \tag{3}$$

$$g_i^{(eq)} = \omega_i T\left[1 + \frac{(C_i.u)}{C_s^2}\right] \tag{4}$$

$$\rho = \sum_i f_i, \rho u = \sum_i c_i f_i, T = \sum_i g_i \tag{5}$$

$$\omega_0 = \frac{4}{9},\ i = 9$$

$$\omega_i = \frac{1}{9},\ i = 1,2,3,4 \tag{6}$$

$$\omega_i = \frac{1}{36},\ i = 5,6,7,8$$

$$c_0 = 0,\quad i = 9$$

$$c_i = \left\{\cos\left[\frac{\pi}{2}(i-1)\right], \sin\left[\frac{\pi}{2}(i-1)\right]\right\},\ i = 1,2,3,4$$

$$c_i = \sqrt{2}\left\{\cos\left[\frac{\pi}{2}(i-5)+\frac{\pi}{4}\right], \sin\left[\frac{\pi}{2}(i-5)+\frac{\pi}{4}\right]\right\},\ i = 5,6,7,8 \tag{7}$$

$$F_i = F_y \tag{8}$$

$$F_y = -3\omega_i p v H a^2 \mu / H^2 + 3 w_i g \rho \beta \theta$$

$$\tau_c = \frac{\alpha}{C_s^2 \Delta t} + 0.5, \tau_v = \frac{v}{C_s^2 \Delta t} + 0.5 \tag{9}$$

$$X = \frac{x}{H}, Y = \frac{y}{H}, U = \frac{uH}{\alpha_f}, V = \frac{vH}{\alpha_f}, \theta = \frac{T - T_c}{T_h - T_c}$$

$$Pr = \frac{\vartheta_f}{\alpha_f},\ Gr = \frac{g\beta_f H^3 (T_h - T_c)}{{\vartheta_f}^2}, Ha = B_0 H\sqrt{\frac{\sigma_f}{\mu_f}}, Re = \frac{U_0 H}{\upsilon_f}, Ri = \frac{Gr}{Re^2} \tag{10}$$

Density, heat capacity, thermal expansion coefficient, heat diffusion

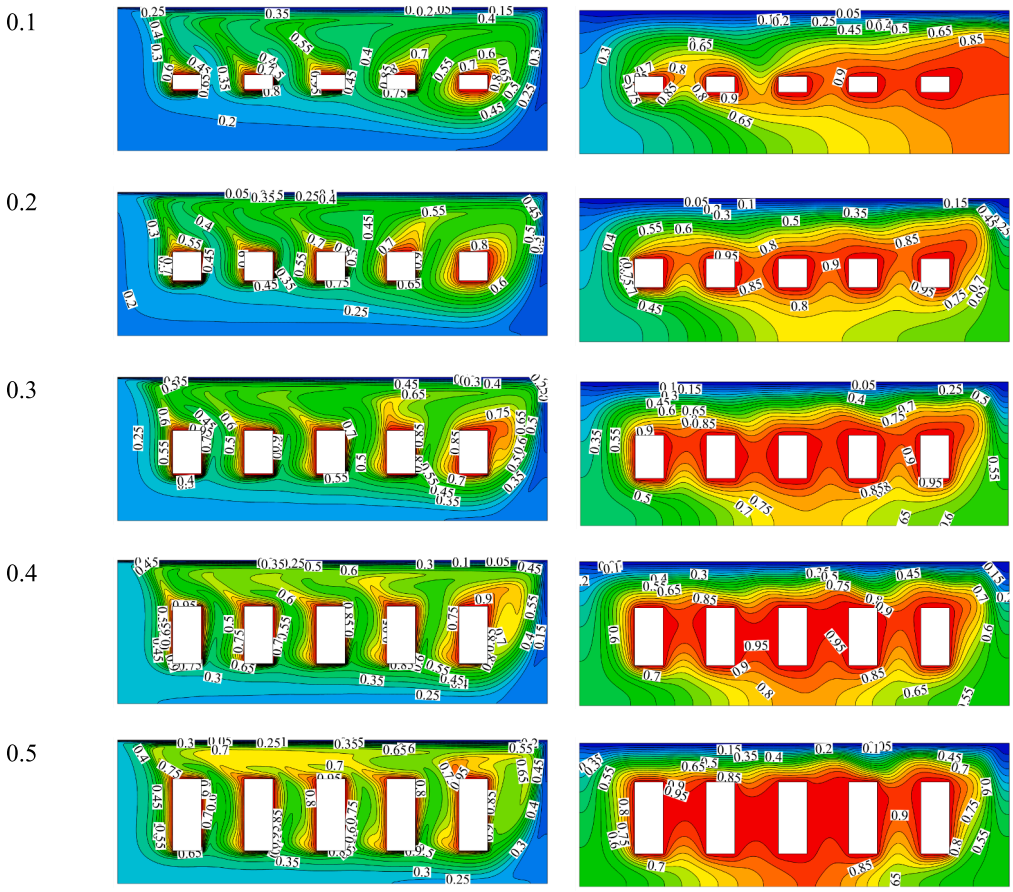

Fig. 6. The contours of isothermal lines for different HOBs and various values of Ri.

coefficient, viscosity, and thermal conductivity are the NF characteristics that may be deduced from Eqs. (11) to (17) [27,28]{Ghasemi, 2011 #1158}. Table 1 provides an overview of the thermophysical characteristics of NPs as well as the base fluid. When it comes to figuring out the rate of HTR, one of the most crucial dimensionless quantities to consider is Nu. The equation (20) is used to calculate the average value of Nu, represented by Nu_{Av}, on the cold wall.

$$\frac{\sigma_{nf}}{\sigma_f} = 1 + \frac{3\left(\frac{\sigma_p}{\sigma_f} - 1\right)\varphi}{\left(\frac{\sigma_p}{\sigma_f} + 2\right) - \left(\frac{\sigma_p}{\sigma_f} - 1\right)\varphi} \tag{11}$$

$$\rho_{nf} = (1-\varphi)\rho_f + \varphi\rho_p \tag{12}$$

$$(\rho C_P)_{nf} = (1-\varphi)(\rho C_P)_f + \varphi(\rho C_P)_p \tag{13}$$

$$(\rho\beta)_{nf} = (1-\varphi)(\rho\beta)_f + \varphi(\rho\beta)_p \tag{14}$$

$$\alpha_{nf} = \frac{k_{nf}}{(\rho Cp)_{nf}} \tag{15}$$

$$\mu_{nf} = \mu_f(1-\varphi)^{-2.5} \tag{16}$$

$$\frac{k_{nf}}{k_f} = 1 + \frac{k_p}{k_f}(1 + cPe)\left\{\frac{d_f}{d_P}\frac{\varphi}{1-\varphi}\right\} \tag{17}$$

$$Pe = u_p d_p/\alpha_f \tag{18}$$

$$u_P = \frac{2k_B T}{\pi\mu_f d_p^2} \tag{19}$$

$$Nu_{Av} = \frac{1}{L}\int_0^1 -\frac{k_{nf}}{k_f}\left(\frac{\partial\theta}{\partial Y}\right)_{Y=H} dX \tag{20}$$

To ensure that the current code is applied correctly to the incompressible domain, the flow velocity length scale for natural convection HTR must be substantially lower than the fluid's sound speed. In this particular piece of research, the typical velocity is assumed to be equal to 0.1 of the speed of sound. It should be pointed out that the kinematic viscosity is calculated according to Eq. (21) when *Gr*, Prandtl number (Pr), and Mach number (Ma) are constant.

$$v_f = \sqrt{pr/Gr}Mac_S H \tag{21}$$

Utilizing the buckling approach, the velocity boundary conditions for smooth walls are modeled. [29]. According to the following illustration, Eq. (22) may be used to determine the temperature and velocity boundary conditions for the vertical wall on the cavity's left side:

$$\begin{aligned} f_1 &= f_3, \\ f_5 &= f_7 \\ f_8 &= f_6 \end{aligned} \tag{22}$$

$$\begin{aligned} g_1 &= T_h(\omega_1 + \omega_3) - g_3 \\ g_8 &= T_h(\omega_8 + \omega_6) - g_6 \\ g_5 &= T_h(\omega_5 + \omega_7) - g_7 \end{aligned} \tag{23}$$

The techniques described by Tao et al. [26] are used in order to do the calculations necessary to determine the velocity and temperature on curved boundaries.

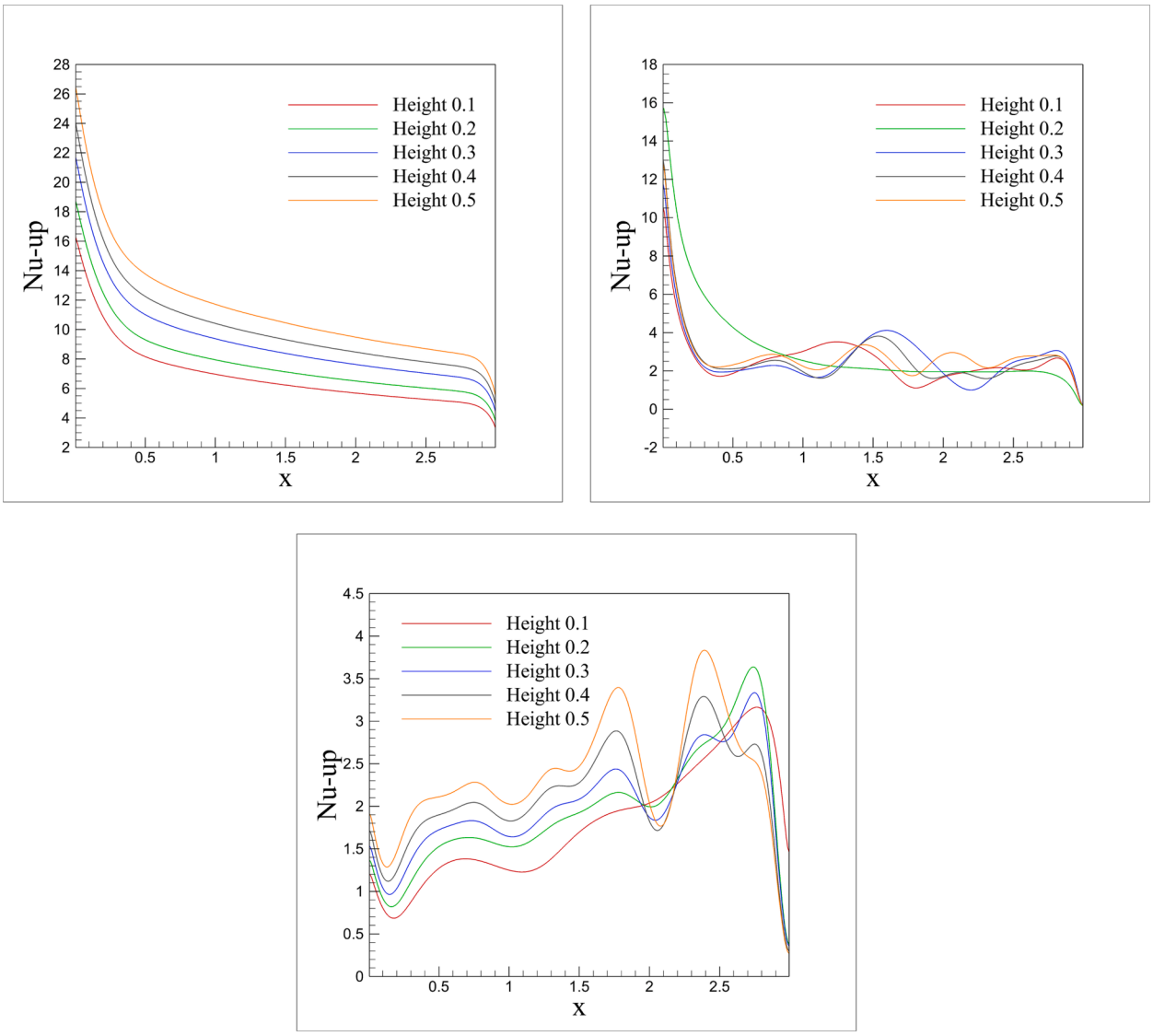

Fig. 7. The value of the local HTR rate on the upper wall in the form of Nu for different HOBs and three different values of Ri.

Grid study and validation

Since the cavity and the obstacles are rectangular, a structured grid is generated on the geometry. Nu_{av} is computed and compared for Ri = 0.01 and 100 for the grids with varied grid points to see whether the findings are independent of the number of grid points (Table 2). According to the obtained results, the grid with 50,000 nodes is selected as the optimal grid.

To verify the obtained results, the results obtained from the simulation of natural convection HTR under the effect of the MCF are compared with Ref. [31] (Table 3) for $Ra = 10^5$, suggesting that there is a high degree of concordance between the previous findings and those described in Reference [31]. This section provides and discusses the simulation results while considering the code's validation and the assurance of the results' accuracy.

Results and discussion

The contours of streamlines and isotherms for various HOBs are shown in Fig. 3. Due to the buoyancy force and shear force produced by the moving wall, weak and tiny vortices are created independently. The vortices are combined by enhancing the HOBs and forming a strong vortex. An increment in the HOBs and moving them towards the upper cold wall leads to forming a vortex in the cavity. Also, examining the isothermal lines demonstrates that the density of the isotherms around the moving wall and heat sources is high. The density of the isotherms around the moving wall rises as the HOBs are improved, and they eventually align with the cold wall. The quantity of conductive HTR is increased, and the amount of convective HTR is decreased when the hot barriers are approached by the cold wall, increasing the density of the isotherms. In this case, the isothermal lines under the obstacles become more regular. Also, the penetration of hot NFs into the lower part of the cavity is reduced with the increase in the HOBs. The approach of the hot obstacles to the cold wall causes the lower part of the cavity to become colder and there is a colder NF in that area. Most of the hot NF is observed between the obstacles. In all cases, the cold NFs move from the right side of the wall towards the bottom of the cavity, and the hot fluid moves from the other side towards the cold wall.

The value of the local Nu on the top wall is examined in Fig. 4 for various HOBs. The spatial HOBs boost the value of Nu at X = 0, and it approaches zero at X = 3. At the beginning of the cold wall, i.e. at X = 0, the value of Nu is high due to the collision of the heated fluid with the obstacles. On the other hand, the value of Nu is relatively low since there is little temperature variation between the NFs and the wall. The cold

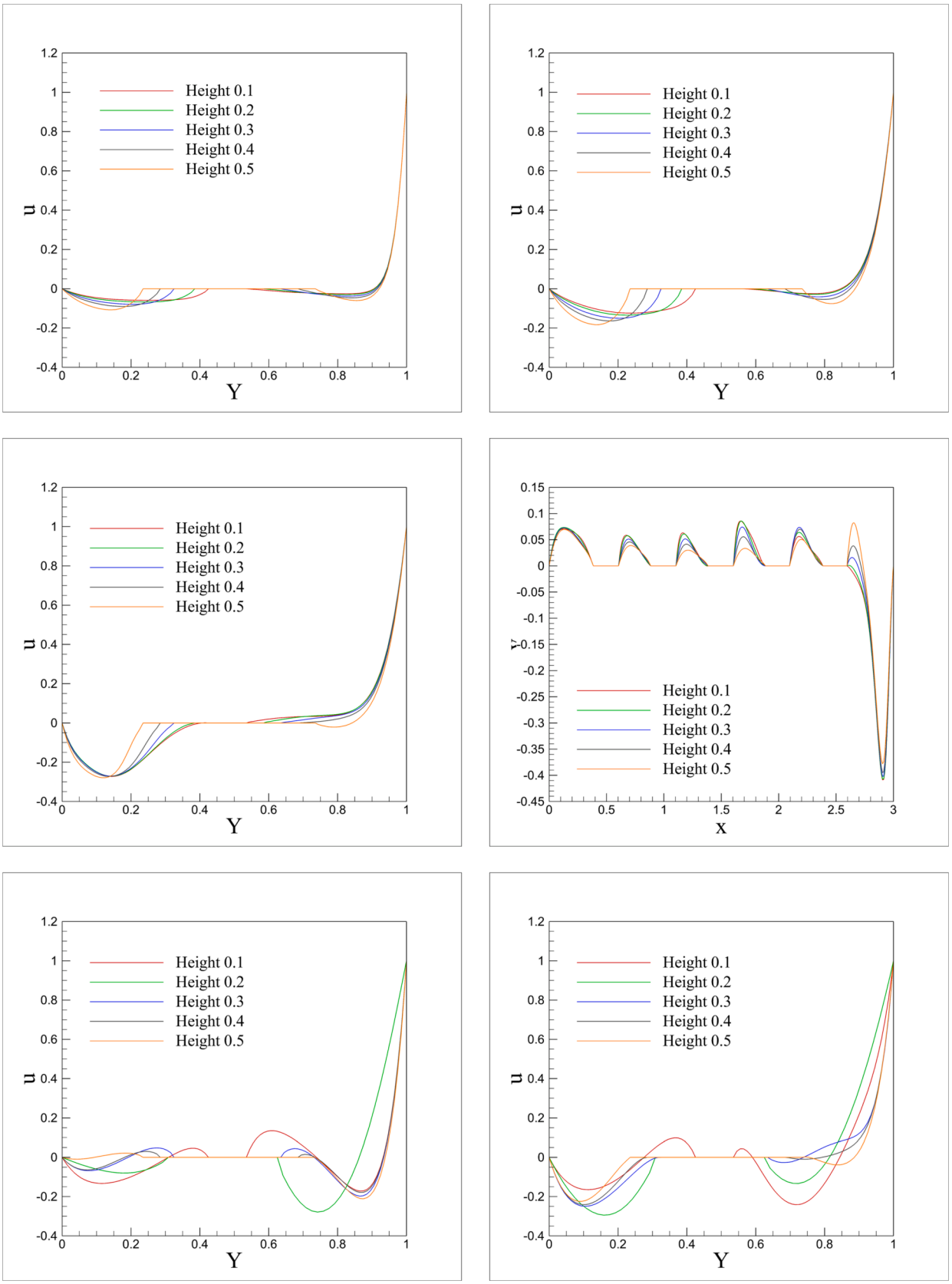

Fig. 8. Shows the profile of the dimensionless horizontal velocity u along the vertical centerline and the profile of the dimensionless horizontal velocity v along the horizontal centerline of the cavity at different HOBs and various Ri values.

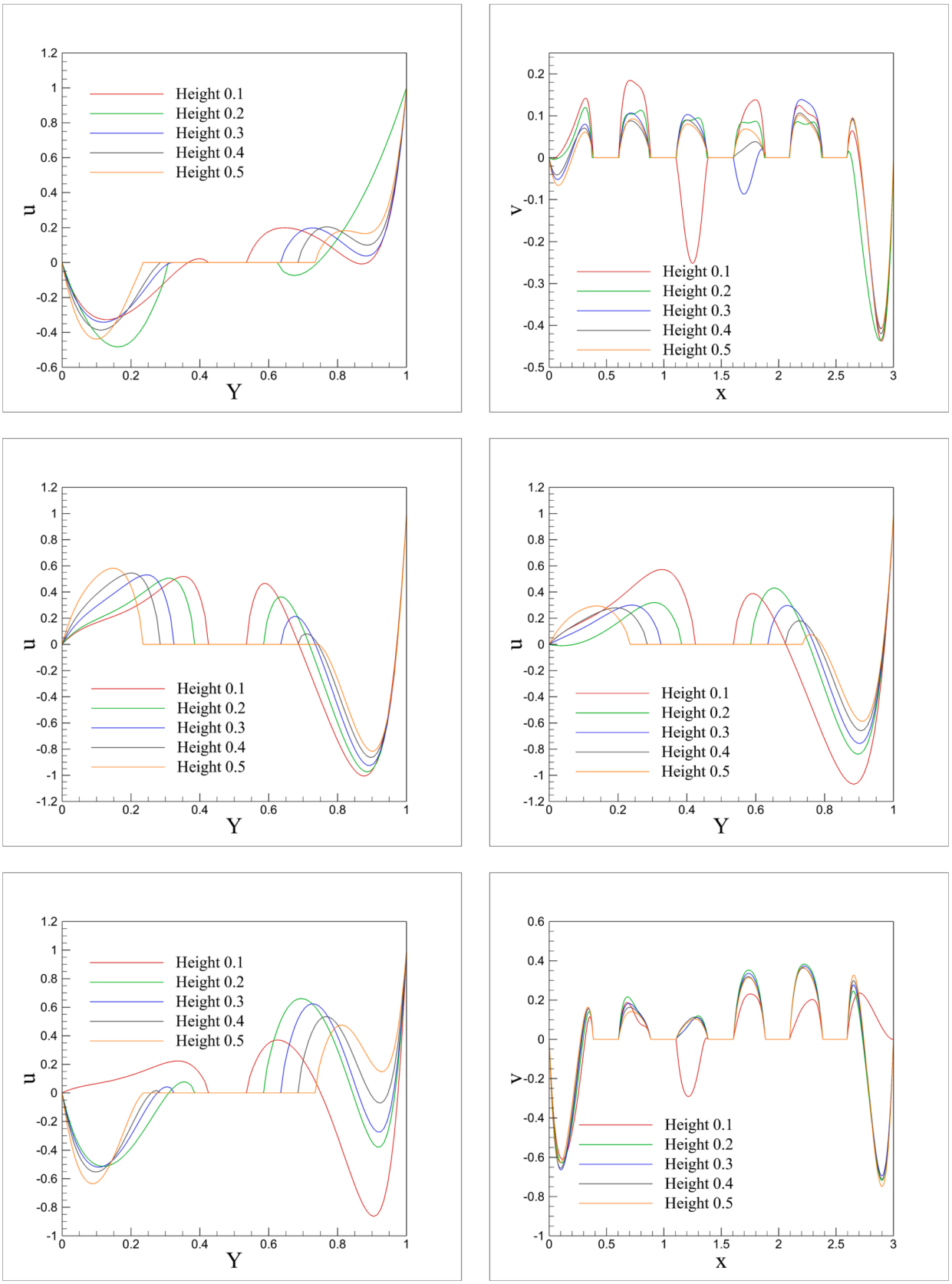

Fig. 8. (*continued*).

NFs exit the cold wall here, causing the Nu to be too tiny. When the heated barriers are at the lowest part of the hollow, the value of Nu on this wall is more linear. However, the value of Nu rises in the locations where the heated barriers are close to the cold wall as they go closer to it.

Table 4 presents the amounts of Nu_{av} on the top wall for different HOBs. It is observed that the Nu_{av} is enhanced with HOB. For the

Table 5
The Nu_{av} of the upper wall for different HOBs and Ri = 0.01, 1and 100.

Ri	HOB	Nu_{a_v}
0.01	0.1	6.86
	0.2	7.85
	0.3	9.21
	0.4	10.23
	0.5	11.44
10	0.1	2.53
	0.2	3.13
	0.3	2.65
	0.4	2.63
	0.5	2.82
100	0.1	1.78
	0.2	1.94
	0.3	2.01
	0.4	2.14
	0.5	2.35

maximum HOBs and in the case where the obstacles are close to the wall, the value of the Nu_{av} is much higher than that in other cases. In the case that the obstacles are closer to the cold wall, due to the increase in conductive HTR in the NFs, the Nu_{av} is much higher. Changing the position of barriers significantly influences conductive HTR but less on convection HTR. The Nuav is increased by the obstructions' close proximity to the cold wall in such a manner that raising the HOBs from 0.25 to 0.4 increases the Nu_{av} value on the cold wall by 44.3 %.

Effect of the HOBs

The streamlines' outlines for various HOBs and Ri values are shown in Fig. 5. It is noted that a vortex forms as a result of the moving wall's shear stress. As the HOBs are enhanced, the vortex becomes stronger so that the velocity gradients between the heat sources increase, and smaller vortices are also formed. As Ri is enhanced, vortices are formed inside the cavity separately. The density of the center of these vortices is higher in the areas above the heat sources. By enhancing Ri, the strength and shape of these vortices become the same so that at Ri = 100, several individual rotating vortices with almost the same shape are formed in the cavity. At low Ri values, the effect of the motion of the cold wall on the formation of vortices is more significant. By increasing the Ri, the impact of the movement of this wall on the vortices is decreased, and the buoyancy force causes the formation of the vortices inside the cavity. The buoyancy force and the number of NFs in the cavity both rise as the barriers grow, which has a detrimental influence on the vortex strength. The whole cavity is occupied by the robust vortex that was created at low Ri values. High Ri concentrations result in more vortices, which lessens the effect of forced convection in the cavity.

Fig. 6 depicts the contours of isothermal lines for different HOBs and various values of Ri. As can be seen, the density of the isothermal lines around the hot sources and the cold wall is high. As the HOBs and their size are enhanced, the thickness of the isothermal lines around the moving wall is increased. The high-temperature gradients close to this wall may cause the thin thermal boundary layers along the higher walls. The density of the isothermal lines around heat sources increases when the Ri is reduced. The flow in the cavity is higher for low values of Ri because of the strong convection effect of the top wall, and as a consequence, the isotherms density on the upper wall and the barriers are high. The top wall's convection power decreases when the Ri is increased. As a result, the vortex is weaker, and the buoyancy force is primarily responsible for producing the vortex. Consequently, there is a decrease in the density of isothermal lines on the cold wall and hot barriers.

The effect of Ri and the HOBs on the HTR rate is now examined. Fig. 7 illustrates the value of the local HTR rate on the upper wall in the form of Nu for different HOBs and three different values of Ri. At Ri = 0.01, the maximum value of Nu occurs around the x = 0. It is enhanced with the increase in HOB. Enhancing the X reduces its value until it reaches its minimum value at the end of the wall. As the Ri is intensified, the amount of Nu is reduced with an oscillatory state. At low Ri values, the graph is without oscillation, and the Nu varies with the HOBs as parallel lines. At high values of Ri, especially Ri = 100, increasing the HOBs has different effects on Nu at different amounts of X. It is clear that an increase in HOBs generally results in a minor rise in the quantity of Nu on the cold wall. By increasing the HOBs at higher values of Ri, i.e., stronger convection flow, there is a more significant increase in the Nu in the areas where the obstacles are located.

As the HOBs and Ri are varied, Fig. 8 depicts the profile of the dimensionless horizontal velocity u along the vertical centerline and the profile of the dimensionless horizontal velocity v along the horizontal centerline of the cavity. As you can see, in all vertical profiles, the velocity is zero in Y = 0, and the velocity tends to be the lid velocity in Y = 1. In other intervals, the zero range is increased as the HOB of the interval increases. The negative value of U in Y indicates the presence of flow that is traveling in the opposite direction to the direction the lid is moving. Additionally, the velocity is zero across a range of HOB. As the BH increases, the range of zero value approaches the moving wall. There is no velocity at x = 0 and x = 3. For x between 2.5 and 3, there is also a clear trend toward decreasing values. The velocity on all velocity charts zeros out in the vicinity of the obstacles. The areas where there is zero velocity in the hollow are affected by changes in the HOBs. Due to the reduced forced convection effect in the cavity caused by a rise in Ri, the NFs' horizontal and vertical velocities are decreased.

Table 5 provides the Nu_{av} of the upper wall for different HOBs and Ri = 0.01, 1and 100. The Nu_{av} is enhanced with the HOBs. As Ri increases, the Nu_{av} decreases. By improving the HOBs, the cavity has more hot walls so that the NFs can contact them. The quantity of HTR on the cold wall is amplified because the temperature of the NFs is rising, which increases the temperature differential between them and the cold wall. This is especially valid for low values of Ri. Enhancing the HOBs from 0.1 to 0.5 intensifies the Nu_{av} by 66.7, 11.4, and 32 %, for Ri = 0.01, 1, and 100, respectively. When the convection in the cavity is stronger, the effect of increasing the HOBs on the Nu_{av} is more significant. The quantity of HTR that is present on the cold wall decreases due to an increase in Ri brought on by a reduction in the effect of wall movement on the flow of the NFs. The increment in the Ri decreases by 74 % and 79.4 % in the Nu_{av} when the HOBs are small and large, respectively.

Conclusions

This study employs the Lattice Boltzmann Method (LBM) to model mixed nanofluid (NF) convection in a rectangular cavity. The cavity configuration comprises five high-temperature barriers (HOBs), a movable cold wall, and three insulated walls. A constant magnetic field (MCF) influences the domain. By varying the positions of the HOBs, the locations of obstacles, and the Richardson number (Ri), we obtain the following key results:

- Increasing the height of the HOBs (HOBs) leads to a substantial rise in the average Nusselt number (Nuav). Specifically, when the HOBs are elevated from 0.1 to 0.5, the Nuav increases by 66.7 %, 11.4 %, and 32 % for Ri values of 0.01, 1, and 100, respectively.
- Elevating the Richardson number (Ri) is associated with reducing the average Nusselt number (Nu_{av}) on the cold wall. The increase in Ri decreases 74 % and 79.4 % in the Nuav when the HOBs are set to both small and large values, respectively.
- Increasing the height of the HOBs from the bottom wall yields a notable enhancement in the Nuav. Specifically, an increase from 0.25 to 0.4 in HOB height results in a significant 44.3 % boost in the Nu_{av} on the cold wall.

- The maximum Nu value is observed near x = 0. As the position along the x-axis (X) increases, the Nu value gradually decreases until it reaches its minimum value at the end of the wall.

CRediT authorship contribution statement

Jawed Mustafa: Investigation, Methodology, Writing – original draft, Writing – review & editing, Data curation, Project administration. **Saeed Alqaed:** Investigation, Writing – review & editing, Writing – original draft. **Shahid Husain:** Investigation, Writing – original draft, Writing – review & editing. **Mohsen Sharifpur:** Investigation, Project administration, Resources, Writing – review & editing.

Declaration of competing interest

The authors declare that they have no known competing financial interests or personal relationships that could have appeared to influence the work reported in this paper.

Data availability

Data will be made available on request.

Acknowledgment

Authors would like to acknowledge the support of the Deputy for Research and Innovation Ministry of Education, Kingdom of Saudi Arabia for this research through a grant (NU/IFC/2/SERC/-/22) under the Institutional Funding Committee at Najran University, Kingdom of Saudi Arabia.

References

[1] Kuznik F, Vareilles J, Rusaouen G, Krauss G. A double-population lattice Boltzmann method with non-uniform mesh for the simulation of natural convection in a square cavity. Int J Heat Fluid Flow 2007;28(5):862–70.
[2] Kao PH, Yang RJ. Simulating oscillatory flows in Rayleigh-Bénard convection using the lattice Boltzmann method. Int J Heat Mass Transf 2007;50(17):3315–28.
[3] Ramian P, Rahni MT, Adamian A. Computational simulation of effects of nano-fluidicity and flow boundaries on natural heat transfer in presence of magnetic field, using LBM. Modares Mech Eng 2015;15(6).
[4] Ghasemi K, Siavashi M. Three-dimensional analysis of magnetohydrodynamic transverse mixed convection of nanofluid inside a lid-driven enclosure using MRT-LBM. Int J Mech Sci 2020;165:105199.
[5] Sajjadi H, et al. Simulation of three dimensional MHD natural convection using double MRT Lattice Boltzmann method. Physica A 2019;515:474–96.
[6] Aliu O, Sakidin H, Foroozesh J, Yahya N. Lattice Boltzmann application to nanofluids dynamics-A review. J Mol Liq 2020;300:112284.
[7] Frisch U, Hasslacher B, Pomeau Y. Lattice-Gas automata for the Navier-Stokes equation. Phys Rev Lett 1986;56(14):1505–8.
[8] Higuera FJ, Jiménez J. Boltzmann approach to lattice gas simulations. Europhys Lett (EPL) 1989;9(7):663–8.
[9] Chen H, Chen S, Matthaeus WH. Recovery of the Navier-Stokes equations using a lattice-gas Boltzmann method. Phys Rev A 1992;45(8):R5339–42.
[10] Kefayati GR, Tang H. MHD thermosolutal natural convection and entropy generation of Carreau fluid in a heated enclosure with two inner circular cold cylinders, using LBM. Int J Heat Mass Transf 2018;126:508–30.
[11] Asadi AM, et al. Heat transfer enhancement inside channel by using the Lattice Boltzmann Method. Therm Sci 2021;25(5 Part A):3543–55.
[12] Kolsi L, et al. Impacts of double rotating cylinders on the forced convection of hybrid nanofluid in a bifurcating channel with partly porous layers. Case Stud Therm Eng 2021;26:101020.
[13] Kosinska A, Balakin BV, Kosinski P. Use of biodegradable colloids and carbon black nanofluids for solar energy applications. AIP Adv 2021;11(5):055214.
[14] Kumar K, Chauhan PR, Kumar R, Bharj RS. Irreversibility analysis in Al_2O_3-water nanofluid flow with variable property. Facta Universitatis, Ser: Mech Eng 2022;20 (3):503–18.
[15] Vahedi SM, Aghakhani S, Pordanjani AH, Azaiez J. A comprehensive parametric study on heat transfer optimization of a triangular enclosure subjected to a magnetic field using neural network machine learning. Eng Anal Bound Elem 2022; 145:173–86.
[16] Körpinar T, Körpinar Z. Spherical electric and magnetic phase with Heisenberg spherical ferromagnetic spin by some fractional solutions. Optik 2021;242:167164.
[17] He J-H, Moatimid GM, Sayed A. Effect of mass and heat transfer on EHD stability of two dusty liquid layers between two inclined rigid plates. Int J Mod Phys B 2023: 2450013.
[18] Zhou J, Ali MA, Alizadeh A, Sharma K. Numerical study of mixed convection flow of two-phase nanofluid in a two-dimensional cavity with the presence of a magnetic field by changing the height of obstacles with artificial intelligence: Investigation of entropy production changes and Bejan number. Eng Anal Bound Elem 2023;148:52–61.
[19] Ketchate CGN, Kapen PT, Fokwa D, Tchuen G. Stability analysis of mixed convection in a porous horizontal channel filled with a Newtonian Al_2O_3/Water nanofluid in presence of magnetic field and thermal radiation. Chin J Phys 2022; 79:514–30.
[20] Abderrahmane A, et al. Analysis of mixed convection of a power-law non-Newtonian nanofluid through a vented enclosure with rotating cylinder under magnetic field. Ann Nucl Energy 2022;178:109339.
[21] Akhter R, Ali MM, Billah MM, Uddin MN. Hybrid-nanofluid mixed convection in square cavity subjected to oriented magnetic field and multiple rotating rough cylinders. Results Eng 2023;18:101100.
[22] Philip J. Magnetic nanofluids (Ferrofluids): Recent advances, applications, challenges, and future directions. Adv Colloid Interface Sci 2023;311:102810.
[23] Wang J, et al. A review on nanofluid stability: preparation and application. Renew Sustain Energy Rev 2023;188:113854.
[24] Mohamad AA. Lattice Boltzmann method: fundamentals and engineeringapplications with computer codes. London: Springer London; 2019. https://doi.org/10.1007/978-1-4471-7423-3.
[25] Bhatnagar PL, Gross EP, Krook M. A model for collision processes in gases. I. Small amplitude processes in charged and neutral one-component systems. J Physical Review 1954;94(3):511–25.
[26] Tao S, et al. A curved lattice Boltzmann boundary scheme for thermal convective flows with Neumann boundary condition. Int J Heat Mass Transf 2020;150: 119345.
[27] Patel HE, Anoop K, Sundararajan T, Das SK. *A micro-convection model for thermal conductivity of nanofluids*. in *International Heat Transfer Conference 13*. 2006. Begel House Inc.
[28] Brinkman HC. The viscosity of concentrated suspensions and solutions. J Chem Phys 1952;20(4):571.
[29] Girimaji, S., Lattice Boltzmann Method: Fundamentals and Engineering Applications with Computer Codes. 2013;**51**(1):278-9.
[30] Khodadadi H, et al. A comprehensive review on rheological behavior of mono and hybrid nanofluids: Effective parameters and predictive correlations. Int J Heat Mass Transf 2018;127:997–1012.
[31] Sathiyamoorthy M, Chamkha A. Effect of magnetic field on natural convection flow in a liquid gallium filled square cavity for linearly heated side wall(s). Int J Therm Sci 2010;49(9):1856–65.